Nanoscale

PAPER

View Article Online
View Journal | View Issue

Cite this: *Nanoscale*, 2016, **8**, 16357

Controlling the rectification properties of molecular junctions through molecule–electrode coupling†

Matthieu Koepf,‡§[a] Christopher Koenigsmann,¶‡[a] Wendu Ding,‖[a] Arunbah Batra,[b] Christian F. A. Negre,[c] Latha Venkataraman,*[b] Gary W. Brudvig,*[a] Victor S. Batista,*[a] Charles A. Schmuttenmaer*[a] and Robert H. Crabtree*[a]

Received 16th June 2016,
Accepted 16th August 2016

DOI: 10.1039/c6nr04830g

www.rsc.org/nanoscale

The development of molecular components functioning as switches, rectifiers or amplifiers is a great challenge in molecular electronics. A desirable property of such components is functional robustness, meaning that the intrinsic functionality of components must be preserved regardless of the strategy used to integrate them into the final assemblies. Here, this issue is investigated for molecular diodes based on *N*-phenylbenzamide (*N*PBA) backbones. The transport properties of molecular junctions derived from *N*PBA are characterized while varying the nature of the functional groups interfacing the backbone and the gold electrodes required for break-junction measurements. Combining experimental and theoretical methods, it is shown that at low bias (<0.85 V) transport is determined by the same frontier molecular orbital originating from the *N*PBA core, regardless of the anchoring group employed. The magnitude of rectification, however, is strongly dependent on the strength of the electronic coupling at the gold–*N*PBA interface and on the spatial distribution of the local density of states of the dominant transport channel of the molecular junction.

1. Introduction

The development of robust molecular components functioning as components of molecular integrated circuits is a primary goal of molecular electronics.[1–4] Ultimately, nano-sized components could permit the assembly of advanced sensors, logic gates, or energy conversion devices.[5] An essential component for any such developments is the single molecule rectifier (or molecular diode).[6]

The implementation of molecular components into functional devices will require a detailed understanding of the fundamental relationship between the intrinsic performance of the component considered and the strategy used to interface it to the surrounding device architecture. Here, we investigate the influence of metallic contacts on the rectification properties of archetypal gold–diode–gold molecular junctions.

We focus on *N*-phenylbenzamide (*N*PBA) derivatives since earlier studies have indicated that they are good candidates for intrinsic rectification.[7] Furthermore, they offer a stable molecular backbone of which the substitution pattern can be systematically tailored using robust synthetic strategies. Finally, their structural simplicity makes them accessible to advanced computational analysis and combinatorial methods for a detailed understanding of their electronic properties.[7–9]

From an experimental perspective, the Scanning Tunneling Microscopy Break-Junction (STM-BJ)[10,11] technique has enabled direct investigation of the transport properties of such derivatives.[12] In these measurements, the selected molecular backbone is interfaced with nanoscopic metallic electrodes (typically gold electrodes) *via* specific chemical functionalities that act as anchoring groups. In the case of simple molecular

[a]*Department of Chemistry & Energy Sciences Institute, Yale University, P.O. Box 208107, New Haven, Connecticut 06520-8107, USA. E-mail: gary.brudvig@yale.edu, victor.batisa@yale.edu, charles.schmuttenmaer@yale.edu, robert.crabtree@yale.edu*
[b]*Department of Applied Physics and Applied Mathematics, Columbia University, Mail Code: 4701, New York, NY 10027, USA. E-mail: lv2117@columbia.edu*
[c]*Theoretical Division, Los Alamos National Laboratory, Los Alamos, New Mexico 87545, USA*

†Electronic supplementary information (ESI) available: Detailed synthetic procedures and full characterization of the derivatives; description of the leads used in the theoretical studies; details of the parameters used for the single state tight binding model; representation of the DOS of the three junctions; representation of the HOMO and LUMO state of an isolated *N*PBA backbone; determination of the angular dependence of the PDOS of the phenyl/anchor–lead fragments; and ^{1}H, ^{13}C ^{19}F NMR spectra of the derivatives. See DOI: 10.1039/c6nr04830g

‡These authors contributed equally to this work.
§Current address: Laboratoire de Chimie et Biologie des Métaux, CEA-CNRS-UGA UMR 5249, 17 avenue des martyrs 38054 Grenoble Cedex 9, France.
¶Current address: Department of Chemistry, Fordham University, 441 East Fordham Road, Bronx, NY 10458, USA.
‖Current address: Department of Chemistry, Northwestern University, 2145 Sheridan Road, Evanston, IL 60208-3113, USA.

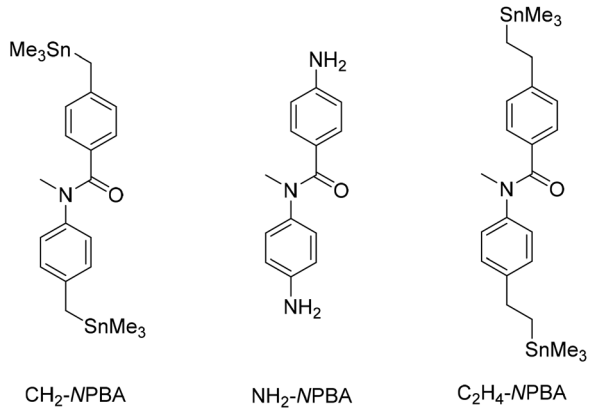

Fig. 1 Schematic drawing of the three *N*PBA derivatives investigated in this work.

wires, it has been shown that the nature of the anchoring groups can be of critical importance in determining the molecular states that govern the transport through the junction, and in controlling the strength of the electronic coupling between the backbone and the electrode materials.[13]

Rectification has been observed in molecular wires possessing symmetrical unsaturated backbones when different anchoring groups were employed on opposite termini of the wire, leading to a difference in the coupling to the gold leads.[14,15] In molecular diode motifs with intrinsically asymmetric backbones, rectification is achieved even with symmetrical anchoring groups.[16,17] Thus, a key question arises: how does coupling in symmetrically anchored metal–molecule–metal junctions influence the electronic properties and intrinsic rectification of molecular diodes such as *N*PBA derivatives? To address this question, we synthesized and analyzed a series of *N*PBA derivatives symmetrically substituted with a range of anchoring groups (Anchor–*N*PBA–Anchor, Anchor = CH_2, NH_2, or C_2H_4, Fig. 1).

We studied the transport properties of the gold–*N*PBA–gold junctions by using a combined experimental and computational approach that allows for interpretation of STM-BJ measurements based on density functional theory (DFT) calculations, the non-equilibrium Green's function (NEGF) approach and a single-state tight-binding model based on the Breit–Wigner formula.[18] Our findings demonstrate that within the range of bias considered (<0.85 V) the dominant transport channel of the junctions and the rectification mechanism remain the same throughout the series of *N*PBA derivatives, despite the changes in anchoring groups. However, for any given bias, the anchoring group significantly affects the experimentally determined conductance and magnitude of rectification.

2. Methods

STM break-junction measurements (STM-BJ)

The molecular conductance and current–voltage (*I*–*V*) characteristics were obtained utilizing a scanning tunneling microscope (STM) in the break-junction mode.[11,14] The break-junction technique relies on forming and breaking gold point contacts within a solution of the molecules of interest. A freshly cut gold wire (0.25 mm diameter, 99.999%, Alfa Aesar) and a mica disk coated with 100 nm of gold (99.999%, Alfa Aesar) were employed as the STM tip and substrate, respectively. The gold coated substrate was pre-treated in an UV-ozone etcher to remove residual organic impurities immediately before performing STM experiments. The STM break-junction measurements were performed under ambient, room temperature conditions. Initially, ~1000 conductance traces are collected with the pristine gold tip and substrate in order to verify that the tip and substrate are free of contaminants.

The conductance and *I*–*V* characteristics of the single molecule contacts are subsequently measured by forming junctions in the presence of a dilute solution of the desired molecule (1 mM–10 mM) dissolved in 1,2,4-trichlorobenzene (99%, Sigma Aldrich).[19] The tip was brought into contact with the surface of the substrate until the conductance was greater than $5G_0$ ($1G_0$ = 77.5 μS). The tip was subsequently withdrawn at a rate of 15 nm s^{-1} for a period of 125 ms and held for a period of 150 ms, while a triangular voltage ramp was applied between +1 V and −1 V. Finally, the tip was withdrawn at 15 nm s^{-1} for a period of 75 ms to break the junction before repeating the process for a total of ~50 000 individual traces. A data selection and sorting process, which is described in detail elsewhere,[14,15] was then employed to generate the histograms of the *I*–*V* curves and determine the average *I*–*V* curve.

Computational methods

The isolated molecules were optimized at the DFT/B3LYP level using the 6-31++G(d,p) basis set as implemented in Gaussian 09 v.C01.[20] The molecular junctions were prepared by inserting the molecular backbones between two gold leads. The latter was modeled by using 6 layers of 16 gold atoms cut from a (111) fcc Au lattice. A gold triad was used to anchor the backbones as shown in Fig. S1.†[7] The geometries of the junctions were optimized using the SIESTA computational package.[21] During optimization the gold atoms forming the core of the leads were kept fixed in space (see the ESI†). The distance between the two leads was systematically varied to find the lowest energy geometry. The latter was used in the computations that followed. Zero-bias conductances were obtained by using the DFT–NEGF approach as implemented in TranSIESTA,[21] with generalized gradient approximation (GGA) functional PBE[22] and with the single-ζ basis set for gold atoms and the double-ζ basis set for the rest of the atoms.[21] A Monkhorst–Pack *k*-point grid of 10 × 10 × 80 was used to sample the Brillouin zone for the gold electrodes and a grid of 10 × 10 × 1 for the molecular region. The energy cutoff for the real space grid was set to 200 Ry. Eigenchannels were computed using INELASTICA as implemented in the SIESTA computational package.[23] Rectification ratios were computed using a single-state tight-binding (TB) model, as described in detail elsewhere,[24] and in the ESI.†

3. Results and discussion

STM break-junction measurements (STM-BJ)

We synthesized the three derivatives **CH_2-*N*PBA**, **NH_2-*N*PBA** and **C_2H_4-*N*PBA**, bearing methyl(trimethylstannyl), amino and ethyl(trimethylstannyl) substituents in the 4,4′ positions, respectively (Fig. 1), to modulate the electronic properties of the interfaces between the gold electrodes and the conjugated *N*PBA backbone. The end-groups were selected to form covalent gold–carbon bonds following the surface-induced cleavage of the trimethylstannyl fragments,[25–27] in the case of **CH_2-*N*PBA** and **C_2H_4-*N*PBA**, or to form purely dative nitrogen–gold bonds[28,29] in the case of **NH_2-*N*PBA**. With **CH_2-*N*PBA** and **NH_2-*N*PBA** derivatives, our specific aim was to probe the effect of the nature of the chemical bonding between the *N*PBA backbone and the electrodes on the properties of the respective junctions; **C_2H_4-*N*PBA** was designed to investigate the consequences of minimizing the direct electronic coupling between the *N*PBA backbone and the anchoring points by adding a second methylene group on each end of the backbone.

All derivatives led to the formation of stable junctions in STM-BJ measurements and the current profiles under both fixed and variable bias were investigated. The distribution of conductances measured under fixed bias (≤0.025 V) for junctions derived from the three *N*PBA derivatives is presented in Fig. 2a. In each case, the average low-bias conductance (G) is determined from a fit of the conductance distribution of the corresponding junction. The G values obtained for the three different anchoring groups are shown in Table 1. The trend is consistent with prior results[12,13] as well as with the theoretically calculated zero-bias conductances (G_{th}) (*vide infra*).

Table 1 Experimentally measured (G) and theoretically predicted (G_{th}) conductances; experimentally determined raw (RR), corrected (RR_c), and predicted (RR_{th}) rectification ratios for **CH_2-*N*PBA**, **NH_2-*N*PBA**, and **C_2H_4-*N*PBA**

Compound	G^a (G_0)	$G_{th}{}^b$ (G_0)	RR[c]	$RR_c{}^d$	$RR_{th}{}^e$
CH_2-*N*PBA	1.0×10^{-3}	6.7×10^{-2}	2.0	1.8	1.8
NH_2-*N*PBA	9.4×10^{-5}	2.2×10^{-5}	1.6	1.4	1.2
C_2H_4-*N*PBA	8.5×10^{-6}	1.6×10^{-5}	1.4	1.2	1.1

[a] Derived from the statistical analysis of STM-BJ traces measured at ≤0.025 V. [b] Determined from DFT–NEGF calculations at zero bias. [c] Derived from the analysis of STM-BJ traces measured under variable bias. The values are reported for 0.80 V. [d] Corrected for the contribution arising from the sorting process of the individual *I–V* curves (*cf.* text). [e] Calculated for an applied bias of 0.80 V.

The rectification ratio (RR) was determined from the asymmetry of the current–voltage (*I–V*) profile. Specifically, the RR is defined as the absolute value of the ratio of the current ($I+$) measured in the positive voltage sweep with respect to the current ($I-$) measured at the same voltage in the negative sweep: $RR = |I+/I-|$. For a fair comparison with the computed values (*vide infra*), at 0.8 V, the raw RR values can be corrected ($RR_c = RR - 0.2$) by removing the contribution that arises from the sorting process of the individual *I–V* curves, which produces a negligible RR of 1.2 in non-rectifying junctions based on *Z*-stillbene.[14] Table 1 summarizes the measured RR and corrected RR_c, at 0.8 V, for the *N*PBA backbones with varying anchoring groups. In agreement with the previous reports,[14,15] we observe an increase in the RR for all junctions upon increasing the applied bias up to 0.8 V (Fig. 2b).

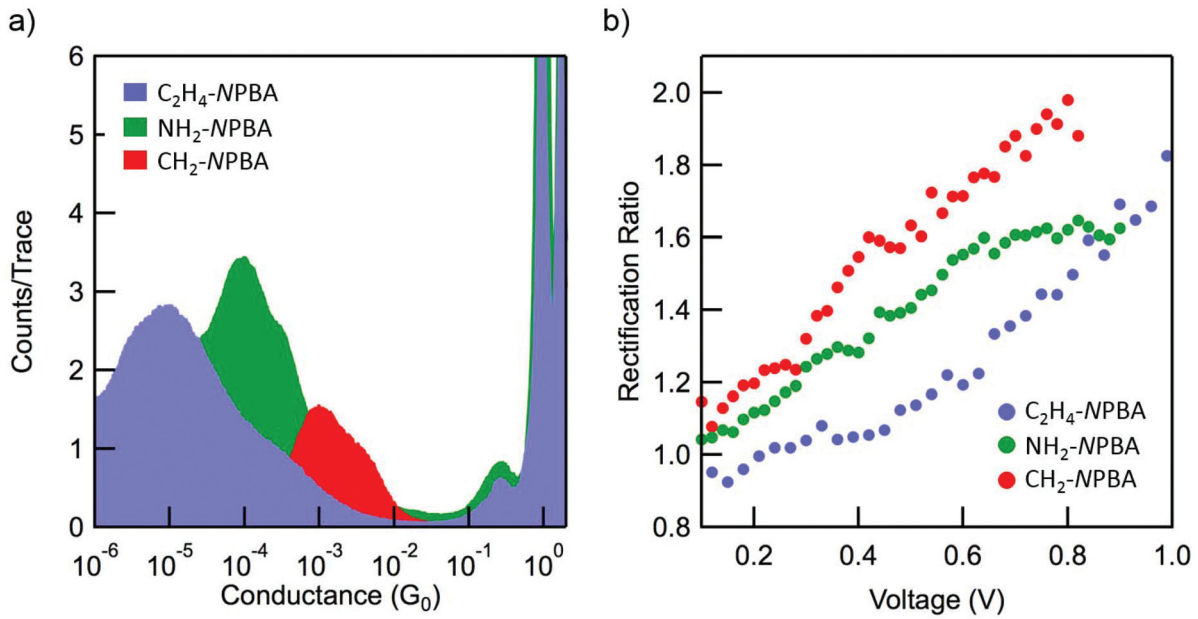

Fig. 2 (a) log-Binned conductance histograms for junctions formed with **CH_2-*N*PBA**, **NH_2-*N*PBA** and **C_2H_4-*N*PBA** between the gold electrodes. (b) Rectification ratio determined as a function of the bias for **CH_2-*N*PBA**, **NH_2-*N*PBA** and **C_2H_4-*N*PBA**.

In the low bias regime (<0.85 V), the increase in the RR was found to correlate with the increase in conductance. The observation of a raw RR of ~2 at 0.8 V, for the junctions derived from **CH_2-*N*PBA** is remarkable in the context of other STM-BJ measurements, especially considering the simplicity of the molecular structure investigated. To the best of our knowledge, it is one of the highest values reported thus far for this method at low bias, for intrinsic rectifiers. As minimal differences in the conformation of the *N*PBA cores are expected within this series, the large variations of conductance and rectification behavior observed among the junctions is most likely related to the modulation of the electronic coupling between the *N*PBA backbone and the metallic electrodes.

Computational analysis

The calculated and experimental values of zero-bias conductance (Table 1) followed the same trend though they differ in the actual magnitude due to the errors inherent to DFT.[29] In all the cases, a single transmission peak (closest to the Fermi level (E_F) of the junction) could be identified as the peak providing the dominant contribution to the transmission function (TF) (see Fig. 3a). By analyzing the local density of states (LDOS) for the three junctions, we identified the state that dominates transport, centered at $E_{NPBA} - E_F = -0.29$, -1.11, and -1.58 eV for **CH_2-*N*PBA**, **C_2H_4-*N*PBA**, and **NH_2-*N*PBA**, respectively (see Fig. S2†).** To support this assignment, the eigenchannels (projection of the eigenvectors of the transmission matrix on the atomic basis set) were computed at the energies mentioned above (see Fig. S3†).[30] We found that the symmetry of the eigenchannels is preserved throughout the series and is reminiscent of the symmetry of the isosurfaces of the LDOS calculated at E_{NPBA} (Fig. 3b–d and S3†). Thus, the latter states contribute significantly to the electron transport through the *N*PBA backbone. The representations of the isosurfaces of the LDOS at E_{NPBA} show strongly asymmetric distributions along the *N*PBA backbones, similarly for the three junctions (Fig. 3b–d). The distributions exhibit a clear homology with the LDOS calculated for the highest occupied molecular orbital (HOMO) of an isolated *N*PBA motif, where the density is mainly centered on the aminophenyl fragment (see Fig. S4†). These observations indicate that the electronic states (centered at E_{NPBA}) that dominate the transport share a common origin in the three junctions and are derived from the HOMO of the *N*PBA backbone. Previous studies have demonstrated that the low-bias rectification properties of *N*PBA derivatives are mainly determined by the asymmetric distribution of the electron density of the HOMO frontier orbital.[7,8] Hence, the HOMO-derived electronic states likely control the transport properties of the junctions under both equilibrium and non-equilibrium regimes. From here on, these states are referred to as the dominant transport channels.

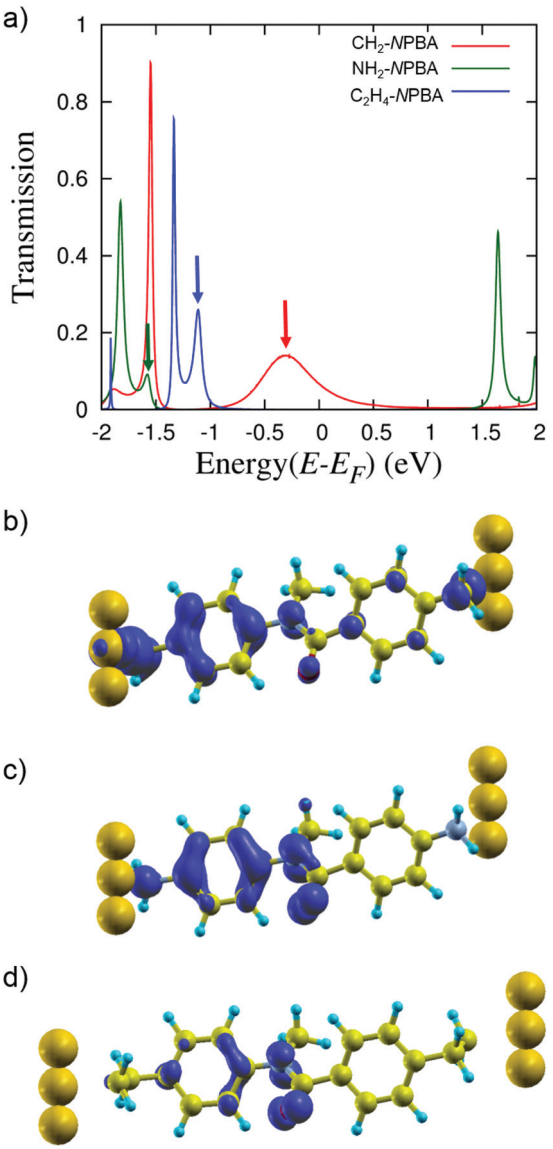

Fig. 3 (a) Overlay of the zero-bias transmission functions (TF) computed for the junctions formed with **CH_2-*N*PBA** (red line), **NH_2-*N*PBA** (green line), and **C_2H_4-*N*PBA** (blue line) derivatives. In each TF the peak closest to the Fermi level (E_F), which dominates the transport properties of the junctions under low bias, is indicated with an arrow. (b), (c) and (d) Representations of the isosurfaces of the local density of state (LDOS) at the energy E_{NPBA} of the electronic state identified as the major contributor to the TF for the junction formed with **CH_2-*N*PBA** (b), **NH_2-*N*PBA** (c) and **C_2H_4-*N*PBA** (d).

To determine the RR under non-equilibrium conditions, we employed a single state tight-binding (TB) model based on the Breit–Wigner formula and computed *I*–*V* curves for the different Au–*N*PBA–Au junctions (see the ESI† for details). The model, parameterized from the zero-bias transmission function (Table S1†), simulates the energy shift of the dominant transport channel (E_{NPBA}), according to the applied bias, and

** In the case of **NH_2-*N*PBA**, a peak centred at +1.65 eV is almost equally distant to E_F than compared to the dominant peak centred in the negative range (−1.58 eV). This suggests that both states might be controlling the transport properties of the junction. However, we will initially focus our analysis on the peak centred at −1.58 eV which nevertheless is the closest in energy to E_F.

provides an approximation of the transport properties of the junctions under non-equilibrium conditions. The TB model provides remarkably good agreement between the RR_{th} and RR_c values (Table 1). These results confirm the critical role of the dominant transport channels identified above in the transport properties of all three junctions.

The nature of the anchoring groups significantly affects the energy alignment and broadening of the TF peaks shown in Fig. 3a, although the dominant transport channel for the three junctions is similar. Thus, the anchoring groups within this series primarily modulate the electronic coupling strength between the gold contacts and the *N*PBA HOMO. The coupling at the interface (as determined from the TB model) increases as follows: $NH_2 < C_2H_4 \ll CH_2$, while the trend observed for both G and RR is: $C_2H_4 < NH_2 \ll CH_2$. The inversion of the order for **C_2H_4-** and **NH_2-*N*PBA** can be rationalized in terms of the efficiency of the coupling between gold and the specific subsets of molecular orbitals that dominate transport (here the π-based HOMO of the *N*PBA backbone; *vide infra*).

First, we focused on the junctions formed by **CH_2-** and **NH_2-*N*PBA**, which share the closest structural similarity in the set. For these junctions, we observe a strong difference in the ability of the gold leads to couple into the π-system of the *N*PBA core, despite the formation of formal σ bonds in each case (either dative N→Au or covalent C–Au bonds). To understand this difference, we examined the ratio of the projected density of states (PDOS) of the phenyl fragment ($PDOS_{Ph}$) to the adjacent Au–anchor motif ($PDOS_{Au-Anchor}$). Specifically, we investigated the variation of the ratio $PDOS_{Ph}/PDOS_{Au-Anchor}$ as the phenyl group is rotated about the axis defined by the anchor–phenyl bond (see Fig. S6 and S7†). In this analysis, a large angle-dependent variation of the ratio $PDOS_{Ph}/PDOS_{Au-Anchor}$ indicates that there is a significant redistribution of the electronic density as the Au–Anchor and phenyl units are rotated with respect to each other from the equilibrium geometry. Such a redistribution can in turn be interpreted as the modulation of the electronic coupling between the Au–Anchor motif and the phenyl π-system, where the more coupled system exhibits the most homogeneously distributed density (*e.g.* PDOS ratio closest to 1).

In the case of **CH_2-*N*PBA**, we observe a significant angle dependence of $PDOS_{Au-Anchor}/PDOS_{Ph}$, with a 7-fold increase of the ratio as the angle varies from +0 to +90° relative to the equilibrium geometry (*cf.* Table S2†). Since a direct π–π overlap is excluded due to the pure sp^3 hybridization of the benzylic carbon, this observation suggests that the strong electronic coupling can be attributed to the hyperconjugation between the quasi-covalent C–Au σ bond and the π-system of the *N*PBA.[31] The electronic interaction between the benzylic C–Au bond and the aromatic π-system, initially postulated[14,26] and recently demonstrated experimentally[25] for (oligo)phenylenes, is thus well captured by our DFT analysis. On the other hand, the **NH_2-*N*PBA**-based junction exhibits a much smaller angle dependence of $PDOS_{Au-Anchor}/PDOS_{Ph}$ with a 2-fold variation of this ratio as the angle is rotated from +0 to +90° from the equilibrium geometry. This is expected since the N→Au dative bond in **NH_2-*N*PBA** is significantly more polarized than the C–Au bond, which reduces the strength of interactions through hyperconjugation.

In the case of **C_2H_4-*N*PBA**, a strong hybridization between the gold leads and the terminal carbons of the backbone accounts for the larger electronic coupling compared to **NH_2-*N*PBA**. However, the π-system of the former remains isolated from the Au–C interface due to the additional methylene group on either side of the backbone. In this case, hyperconjugation cannot occur and the spatial distribution of the local density of states of the dominant transport channel remains strongly localized towards the center of the junction. It results in poorly conductive and virtually non-rectifying junctions in the STM-BJ measurements at low bias.

4. Conclusion

Our results highlight the intimate relationship between the chemical nature of the anchoring groups and the observed electronic properties (conductance and rectification) of molecular junctions built from the *N*PBA molecular diode, in the case of a symmetrically anchored system. This complements earlier reports on the rectification properties of the junctions featuring asymmetrically coupled molecular wires.[14,15,32] In particular, we demonstrate that the RR of a molecular backbone with intrinsic rectification can be enhanced by a suitable choice of the anchors, which in our case reaches a remarkable RR of ~2 as observed in STM-BJ measurements at low bias (<0.85 V). Importantly, we show that variation of the anchoring groups does not fundamentally affect the nature of the dominant transport channel of the *N*PBA-based junctions; however, it affects the coupling into the asymmetrically localized molecular state (HOMO of the *N*PBA backbone) directly responsible for rectification. An important hypothesis stemming from our analysis is that hyperconjugation can play a critical role in allowing for efficient electronic coupling between the gold states and the HOMO level of the *N*PBA backbone, while preserving the essential characteristics of the latter (asymmetrically distributed along the junctions). It is, therefore, natural to conjecture that hyperconjugation, rarely considered in the design of molecular components, may provide an efficient approach to integrate individual molecules into advanced functional assemblies, without compromising the intrinsic properties of the constituent components.

Acknowledgements

We thank the Yale West Campus Analytical Core staff for help with instrumentation. This work was funded by the U.S. Department of Energy Grant DE-FG02-07ER15909 and a generous gift from the TomKat Charitable Trust. V. S. B. acknowledges NERSC support as part of the Argonne-Northwestern Solar Energy Research (ANSER) Center, an Energy Frontier Research Center funded by the U.S.

Department of Energy, Office of Science, Office of Basic Energy Sciences under award no. DE-SC0001059. L. V. thanks the Packard Foundation for support. A. B. was supported by the NSF GRFP Grant No. DGE-07-07425.

Notes and references

1 M. Ratner, *Nat. Nanotechnol.*, 2013, **8**, 378–381.
2 C. Joachim, J. K. Gimzewski and A. Aviram, *Nature*, 2000, **408**, 541–548.
3 J. R. Heath, *Annu. Rev. Mater. Res.*, 2009, **39**, 1–23.
4 R. M. Metzger, *Chem. Rev.*, 2015, **115**, 5056–5115.
5 S. J. van der Molen, R. Naaman, E. Scheer, J. B. Neaton, A. Nitzan, D. Natelson, N. J. Tao, H. van der Zant, M. Mayor, M. Ruben, M. Reed and M. Calame, *Nat. Nanotechnol.*, 2013, **8**, 385–389.
6 W. Ding, C. F. A. Negre, J. L. Palma, A. C. Durrell, L. J. Allen, K. J. Young, R. L. Milot, C. A. Schmuttenmaer, G. W. Brudvig, R. H. Crabtree and V. S. Batista, *ChemPhysChem*, 2014, **15**, 1138–1147.
7 W. Ding, C. F. A. Negre, L. Vogt and V. S. Batista, *J. Chem. Theory Comput.*, 2014, **10**, 3393–3400.
8 W. Ding, M. Koepf, C. Koenigsmann, A. Batra, L. Venkataraman, C. F. A. Negre, G. W. Brudvig, R. H. Crabtree, C. A. Schmuttenmaer and V. S. Batista, *J. Chem. Theory Comput.*, 2015, **11**, 5888–5896.
9 A. Monti, C. F. A. Negre, V. S. Batista, L. G. C. Rego, H. J. M. de Groot and F. Buda, *J. Phys. Chem. Lett.*, 2015, **6**, 2393–2398.
10 B. Q. Xu and N. J. J. Tao, *Science*, 2003, **301**, 1221–1223.
11 M. Kamenetska, M. Koentopp, A. C. Whalley, Y. S. Park, M. L. Steigerwald, C. Nuckolls, M. S. Hybertsen and L. Venkataraman, *Phys. Rev. Lett.*, 2009, **102**, 126803.
12 F. Schwarz and E. Loertscher, *J. Phys.: Condens. Matter*, 2014, **26**, 74201–74201.
13 V. Kaliginedi, A. V. Rudnev, P. Moreno-Garcia, M. Baghernejad, C. Huang, W. Hong and T. Wandlowski, *Phys. Chem. Chem. Phys.*, 2014, **16**, 23529–23539.
14 A. Batra, P. Darancet, Q. Chen, J. S. Meisner, J. R. Widawsky, J. B. Neaton, C. Nuckolls and L. Venkataraman, *Nano Lett.*, 2013, **13**, 6233–6237.
15 A. Batra, J. S. Meisner, P. Darancet, Q. Chen, M. L. Steigerwald, C. Nuckolls and L. Venkataraman, *Faraday Discuss.*, 2014, **174**, 79–89.
16 M. Elbing, R. Ochs, M. Koentopp, M. Fischer, C. von Hänisch, F. Weigend, F. Evers, H. B. Weber and M. Mayor, *Proc. Natl. Acad. Sci. U. S. A.*, 2005, **102**, 8815–8820.
17 I. Diez-Perez, J. Hihath, Y. Lee, L. Yu, L. Adamska, M. A. Kozhushner, I. I. Oleynik and N. Tao, *Nat. Chem.*, 2009, **1**, 635–641.
18 J. C. Cuevas and E. Scheer, *Molecular Electronics: An Introduction to Theory and Experiment*, World Scientific Publishing Company Pte Limited, 2010.
19 J. R. Widawsky, M. Kamenetska, J. Klare, C. Nuckolls, M. L. Steigerwald, M. S. Hybertsen and L. Venkataraman, *Nanotechnology*, 2009, **20**, 434009.
20 M. J. Frisch, G. W. Trucks, H. B. Schlegel, G. E. Scuseria, M. A. Robb, J. R. Cheeseman, G. Scalmani, V. Barone, B. Mennucci, G. A. Petersson, H. Nakatsuji, M. Caricato, X. Li, H. P. Hratchian, A. F. Izmaylov, J. Bloino, G. Zheng, J. L. Sonnenberg, M. Hada, M. Ehara, K. Toyota, R. Fukuda, J. Hasegawa, M. Ishida, T. Nakajima, Y. Honda, O. Kitao, H. Nakai, T. Vreven, J. A. Montgomery Jr., J. E. Peralta, F. Ogliaro, M. Bearpark, J. J. Heyd, E. Brothers, K. N. Kudin, V. N. Staroverov, R. Kobayashi, J. Normand, K. Raghavachari, A. Rendell, J. C. Burant, S. S. Iyengar, J. Tomasi, M. Cossi, N. Rega, J. M. Millam, M. Klene, J. E. Knox, J. B. Cross, V. Bakken, C. Adamo, J. Jaramillo, R. Gomperts, R. E. Stratmann, O. Yazyev, A. J. Austin, R. Cammi, C. Pomelli, J. W. Ochterski, R. L. Martin, K. Morokuma, V. G. Zakrzewski, G. A. Voth, P. Salvador, J. J. Dannenberg, S. Dapprich, A. D. Daniels, Ö. Farkas, J. B. Foresman, J. V. Ortiz, J. Cioslowski and D. J. Fox, *Vol. Revision A.1*, Gaussian, Inc., Wallingford, CT, 2009.
21 M. Brandbyge, J.-L. Mozos, P. Ordejón, J. Taylor and K. Stokbro, *Phys. Rev. B: Condens. Matter*, 2002, **65**, 165401.
22 J. P. Perdew, K. Burke and M. Ernzerhof, *Phys. Rev. Lett.*, 1996, **77**, 3865–3868.
23 https://sourceforge.net/p/inelastica/code/HEAD/tree/.
24 C. Koenigsmann, W. Ding, M. Koepf, A. Batra, L. Venkataraman, C. F. A. Negre, G. W. Brudvig, R. H. Crabtree, V. S. Batista and C. A. Schmuttenmaer, *New J. Chem.*, 2016, DOI: 10.1039/C6NJ00870D, in press.
25 A. Batra, G. Kladnik, N. Gorjizadeh, J. Meisner, M. Steigerwald, C. Nuckolls, S. Y. Quek, D. Cvetko, A. Morgante and L. Venkataraman, *J. Am. Chem. Soc.*, 2014, **136**, 12556–12559.
26 W. Chen, J. R. Widawsky, H. Vazquez, S. T. Schneebeli, M. S. Hybertsen, R. Breslow and L. Venkataraman, *J. Am. Chem. Soc.*, 2011, **133**, 17160–17163.
27 Z. L. Cheng, R. Skouta, H. Vazquez, J. R. Widawsky, S. Schneebeli, W. Chen, M. S. Hybertsen, R. Breslow and L. Venkataraman, *Nat. Nanotechnol.*, 2011, **6**, 353–357.
28 L. Venkataraman, J. E. Klare, C. Nuckolls, M. S. Hybertsen and M. L. Steigerwald, *Nature*, 2006, **442**, 904–907.
29 S. Y. Quek, L. Venkataraman, H. J. Choi, S. G. Louie, M. S. Hybertsen and J. B. Neaton, *Nano Lett.*, 2007, **7**, 3477–3482.
30 M. Paulsson and M. Brandbyge, *Phys. Rev. B: Condens. Matter*, 2007, **76**, 115117.
31 I. V. Alabugin, K. M. Gilmore and P. W. Peterson, *Wiley Interdiscip. Rev.: Comput. Mol. Sci.*, 2011, **1**, 109–141.
32 J. Taylor, M. Brandbyge and K. Stokbro, *Phys. Rev. Lett.*, 2002, **89**, 138301.

